

Time-scale characteristics of Kasai river hydrological regime variability for 1940-1999

Jean-Marie Tshitenge Mbuebue, Albert Mbata Muliwavyo, Vincent Lukanda Mwamba, Edmond Phuku Phuati, Albert Kazadi Mukenga Bantu, and Franck Tondozi Keto

Department of Physics, University of Kinshasa, B.P. 190 Kinshasa XI, DR Congo

Copyright © 2016 ISSR Journals. This is an open access article distributed under the **Creative Commons Attribution License**, which permits unrestricted use, distribution, and reproduction in any medium, provided the original work is properly cited.

ABSTRACT: The present study was undertaken with the aim of contributing to the characterization of the nonstationary variability of the hydrological regime of the Kasai River using the wavelet analysis for 1940-1999. The rainfalls and discharge over Kasai Basin have marked fluctuations with a perceptible downward trend and some shift around 1950, 1960, 1970, 1983 and 1994. The results show that rainfalls over Kasai basin and the discharge at Ilebo station patterns exhibit a strong annual oscillation and some intermittent oscillations in 2-8 years (1950-1975, 1983-1995) and 8-16 years (1970-1999) time scales. The wavelet coherence analysis reveals a weak possible connection between hydrological variables (rainfalls, discharge) and climate indices relative to sea surface temperature and atmospheric circulation over Atlantic tropical, Indian and Pacific Oceans (coherence less than 0.55).

KEYWORDS: wavelet transform, coherence analysis, rainfall, discharge, climate indices.

1 INTRODUCTION

The Kasai river is the chief southern tributary of the Congo River, into which, at Kwamouth, Congo (Kinshasa), 200 km above Malebo (Stanley) Pool, it empties a volume approaching one-fifth that of the main stream. This stretch is interrupted by several spectacular rapids and waterfalls, the river flowing in deeply trenched valleys at elevations of about 600–900 m. The Kasai River eventually crosses a further series of rapids and falls, broadening and deepening to make navigation possible.

For effective and sustainable management of water resources in the Kasai basin the knowledge of their availability and their variability is needed. It is also an important indication for modeling and exploration of the evolution of water resources of this region. In order to improve the understanding of the influence of various factors on the evolution of the hydrological response of the Kasai, and more broadly on the development of water resources, from the regional to a global scale, Kasai watershed has been subject of few studies undertaken by De Backer [1], Devroey [2] who provided a lot of information's about Kasai basin. Ntombi et al. [3] and Kisangala et al. [4] have focused on statistical analyzes based on existing data to establish an understanding of hydrology of the basin.

In the context of climate change, the determination of preferential scales between climate variability and hydrological variability of Kasai watershed is needed. The overall variability of short-term climate is generally associated with phases of oceanic and atmospheric phenomena coupled with El Niño (ENSO) and the North Atlantic Oscillation (NAO). While El Niño Southern Oscillation (ENSO) affects weather and climate variability around the world, the North Atlantic Oscillation (NAO) is the climate dominant mode in the region of the North Atlantic. These oscillations have been used in several studies to develop accurate models able to predict climate variability. The determination of the climate change impact on hydrological systems and their water resources constitutes a major issue of the 21st century for which scientists must answer.

The main objectives are to:

- identify and quantify the main modes of variability of the climate and hydrological response of Kasai river basin;
- characterize the relationships between discharge at Ilebo's station, gridded rainfall over Kasai basin signals and some climate indices.

2 STUDY AREA AND DATA

Kasai basin covers an area of 904,000 square kilometers, between longitudes 15.75 ° and 24.7 ° east and between 0.75 ° South and 12.25 ° South latitude (Fig. 1). 72.4% of this basin is in DR Congo and the remaining 27.6%, representing the Southwest part is located in Angola.

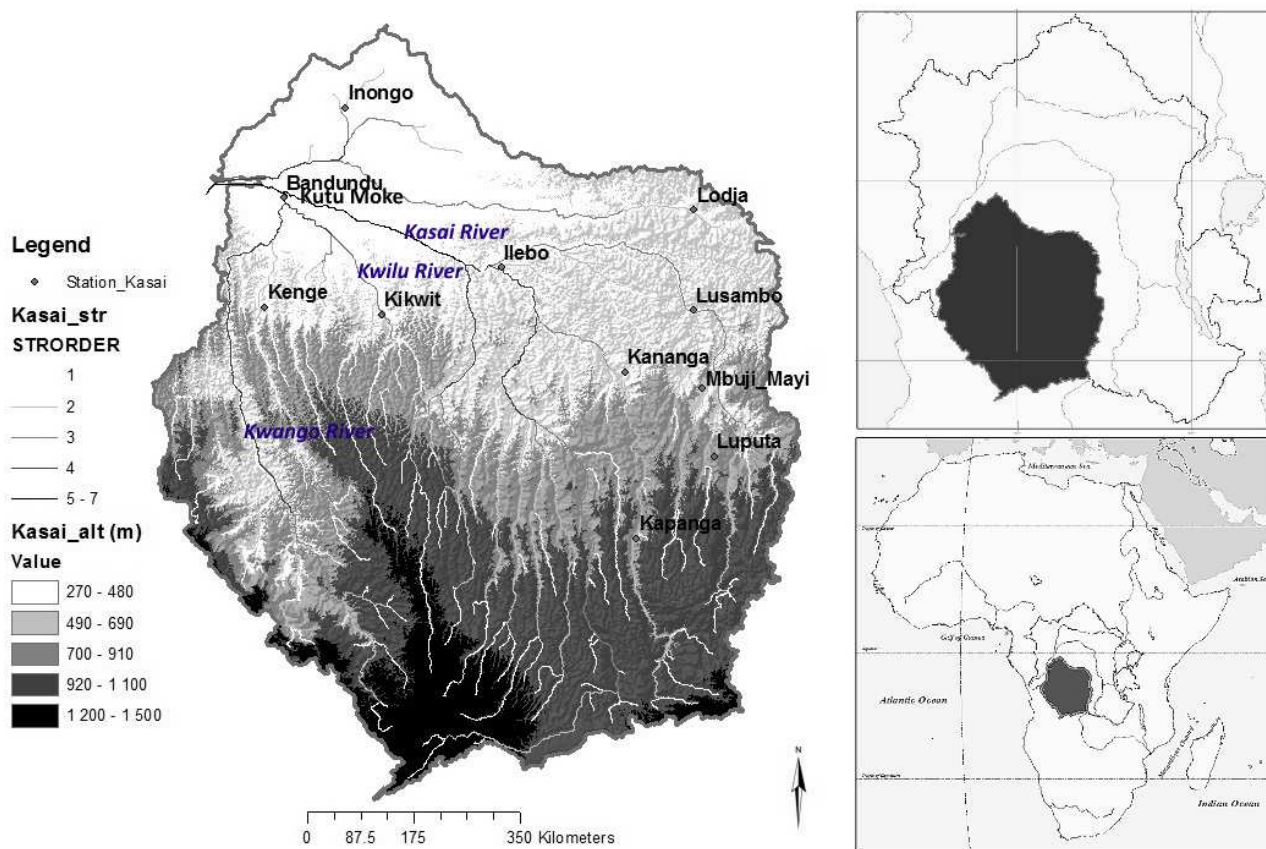


Fig. 1. Relief and stream order map of Kasai watershed

From orographic point of view (Fig. 1), one can identify a depression, sprinkled with few isolated massifs, at the North of the basin around the 4th parallel which is between 300 and 500 meters of altitude. The trays exceeding the altitude of 1000 meters are located on the western edge of the basin between Wamba and Loange, to the south, as well as in the Southeast part. The rapids that cut most of the major tributaries of the basin are located between the plateau at 500 meters of altitude and the central depression.

The longest river in the southern Congo River basin system, the Kasai River, measures 2,153 km from its source on the eastern slope of the Bie Plateau in Angola by 12 ° South and 19 ° East longitude Greenwich, near the plateau 1500 meters above sea level where the Zambezi River also takes its origins [2] to Kwamouth. The Kasai River is the largest tributary of the Congo River. It swells waters of many tributaries whose some of them measure themselves more than 1,000 kilometers.

Its headstream runs east for 250 miles (402 km), then turns north for nearly 300 miles (483 km) to form the frontier between Angola and Congo. Traffic is especially heavy on the 510-mile- (820-kilometre-) long waterway from Kinshasa to Ilebo. Above Ilebo, navigation is impeded by sandbanks, but shallow-draft boats can reach Djokupunda. There the Mai-Munene Falls require goods to be carried 40 miles (64 km) by rail to the next navigable reach, from Mukumbi to Mai-Munene. In its lower reaches, the river enters the equatorial rainforest. Below its confluence with the Kwango, it forms Wissmann Pool and then receives the Fimi-Lukenie, bringing the waters of Lake Mai-Ndombe. Thereafter, it is known as the Kwa.

The climate is equatorial in the northern part of Kasai basin. It is characterized by little difference in seasons, with high temperature and humidity virtually constant. The rainfall distribution throughout the year is on average around 1500 millimeters.

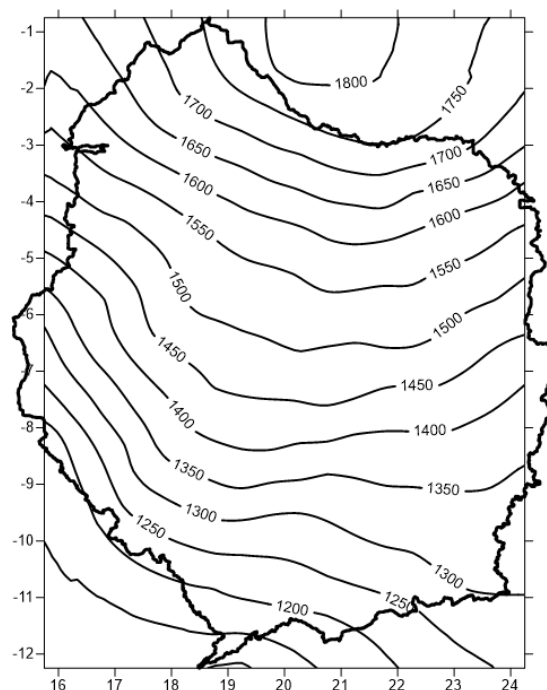


Fig. 2. Mean annual rainfall map of the Kasai basin (1940-1999). Data: SIEREM.v1 at a 0.5°x0.5° resolution. Isohyets in mm.

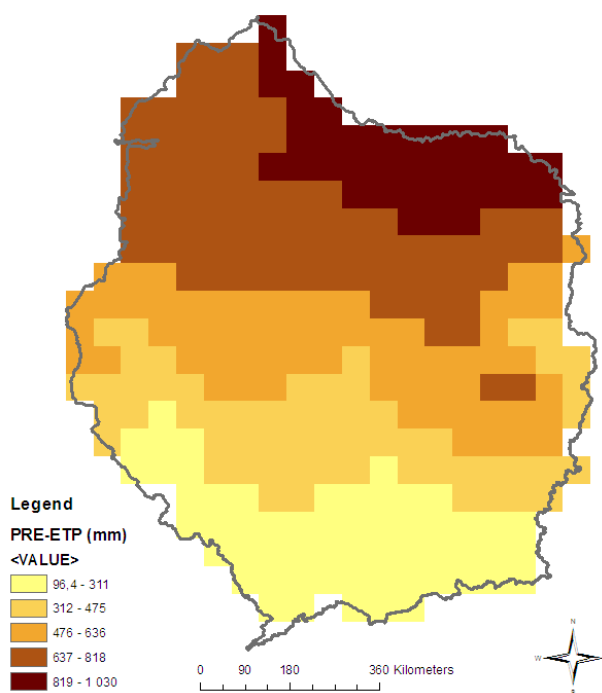


Fig. 3. Rainfalls minus Evapotranspiration (PRE-ETP) map over Kasai watershed the Kasai basin (1940-1999). Data: Climate Research Unit CRU CL 3.10 climatology at a 0.5° resolution (New et al., 2002). Isohyets in mm.

In the South, there is the tropical climate of the Sudan type with two maxima of rainfall and temperature; the dry season becomes longer as one progresses from the north towards the south in the basin. The relief of the southern region of Kasai basin causes a slight temperature drop.

Variations in the length of the rainy season depending on the latitude are clearly demonstrated by the graph in Fig. 6. This basin had 38 weather stations in the colonial era. The mean maximum and minimum absolute temperatures are respectively 32 °/27 °C and 21 °/13 °C in the north/south of Kasai basin (Fig. 4).

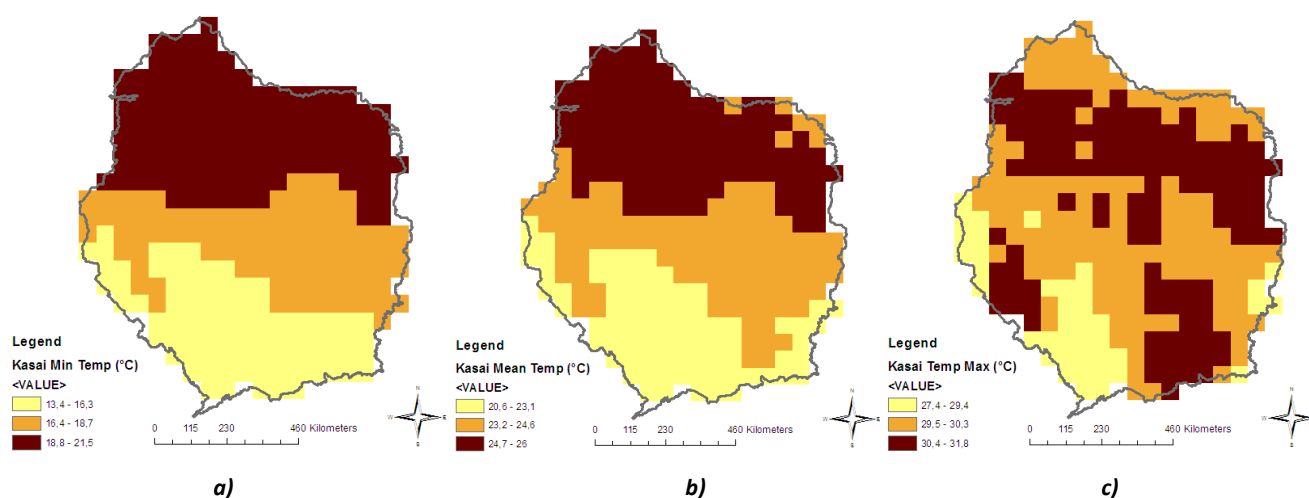


Fig. 4. a) Minimum, b) Mean and c) maximum temperature over Kasai watershed the Kasai basin (1940-1999). Data: Climate Research Unit CRU CL 3.10 climatology at a 0.5° resolution (New et al., 2002). Isohyets in mm.

The great equatorial forest covers just about any depression of the central basin until about the 5th parallel; it pushes its ramifications as wide wooded galleries, going up through the valleys of Kwilu, Kasai and Lulua until the 7th parallel.

Climate data

Gridded rainfall (1940-1999) were extracted from the African gridded data set from the SIEREM database [5] provided by the HydroSciences Montpellier Laboratory on the basis of several data sources, including the former ORSTOM (now IRD – Institut de Recherche pour le Développement) rainfall database [6]. This data set SIEREM.v1 was constructed from SIEREM database by kriging interpolation. SIEREM is an environmental information system for water resources. Raw historical climate datasets are not appropriate for statistical analysis because of inhomogeneity and leakage while gridded datasets have undergone rigorous quality control and have been homogenized [7] [8].

Climate indices used are listed in table 1.

Table 1. Data sources used for monthly climate indices

Climate indices	Data	Periods	Source
NAO	North Atlantic Oscillation [9]	1950-2013	“Earth System Research Laboratory (ESRL) of the National Oceanic and Atmospheric Administration (NOAA)” web page http://www.cpc.ncep.noaa.gov/data/indices/
Nino 3.4	East Central Tropical Pacific SST Index [10]	1951-2013	
TNA	Tropical Northern Atlantic Index [11]	1948-2013	
TSA	Tropical Southern Atlantic Index [11]	1948-2013	
Solar	Solar Flux [12]	1948-2014	
DMI	Dipole Mode Index [13]	1870-2014	The Frontier Research Center for Global Change (JAMSTEC, Japan)” web page (http://www.jamstec.go.jp/frcg/research/d1/iod/HTML/Dipole%20Mode%20Index.html)

3 METHODS

Characterization of the hydrological variability (discharge), the rainfall fluctuations and their comparison with the climate indices are performed by using the signal processing methods (multitaper, wavelet analysis,...).

Climate variability refers to the climatic parameter of a region varying from its long-term mean. Every year in a specific time period, the climate of a location is different. Some years have below average rainfall, others have average or above average rainfall.

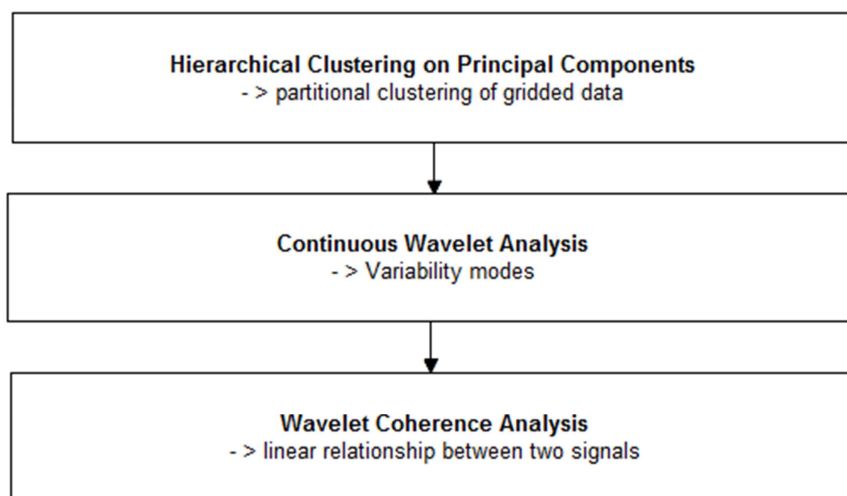


Fig. 5. Diagram of the overall approach of the study

3.1 HIERARCHICAL CLUSTERING ON PRINCIPAL COMPONENTS

Combining principal component methods, hierarchical clustering and partitioning, help to better visualize data and highlight the main features of the data set [14] [15].

3.2 THE SEGMENTATION METHOD OF HILBERT

The time series segmentation procedure in this case gives several changes of average. By using a specific algorithm, one or more shift dates (if any) which separate adjacent segments whose averages have a significant difference under the Scheffe test are selected [16].

3.3 WAVELET TRANSFORM

Recently the wavelet transform has gained a lot of popularity in the field of signal processing. This is due to its capability of providing both time and frequency information simultaneously, hence giving a time-frequency representation of the signal. The traditional Fourier transform can only provide spectral information about a signal. Moreover, the Fourier method only works for stationary signals. In many real world applications, the signals are non-stationary. One solution for processing non-stationary signals is the wavelet transform. The wavelet analysis allows the passage of a representation of a signal to another as Fourier analysis, with a different time-frequency resolution. The wavelet transform $W_n(s)$ of a discrete time series x_n is defined as the convolution of x_n with a scaled and translated version of a function ψ_0 called « mother wavelet » [17]:

$$W_n(s) = \sqrt{\frac{\delta t}{s}} \sum_{n'=0}^{N-1} x_{n'} \psi_0 \left[\frac{(n'-n)\delta t}{s} \right] \tag{1}$$

where δt and s are respectively the time step and the scale.

In this paper, Morlet wavelet is used as « mother wavelet » and consists of a plane wave modulated by a Gaussian:

$$\psi_0(\eta) = \pi^{-1/4} e^{i\omega_0\eta} e^{-\eta^2/2} \tag{2}$$

and ω_0 is taken to be 6 [18].

3.4 GLOBAL WAVELET SPECTRUM (GWS) OR TIME AVERAGE OF LOCAL WAVELET SPECTRA

The Global Wavelet Spectrum (GWS) is used to estimate changes of wavelet power with frequency [19]. It provides an unbiased and consistent estimation of the true power spectrum of a time series. :

It is calculated by:

$$\overline{W}^2(s) = \frac{1}{N} \sum_{n=0}^{N-1} |W_n(s)|^2 \tag{3}$$

3.5 SCALE-AVERAGED WAVELET POWER (SAWP)

The Scale-Averaged Wavelet Power (SAWP), which is defined as the weighted sum of the wavelet power, is used to examine fluctuations in power over a range of a scales (a band). It is given by:

$$\overline{W}_n^2 = \frac{\delta_j \delta_t}{C_\delta} \sum_{j=j_1}^{j_2} \frac{|W_n(s_j)|^2}{s_j} \tag{4}$$

where $C_\delta = 0.776$ for the Morlet wavelet, δ_j is the factor of scale averaging, δ_t is the sampling period, j_1 and j_2 are the scales over which SAWP is computed.

The wavelet –filtered reconstructions of a determined oscillation band-passed, j_1 and j_2 , is given by:

$$X_n = \frac{\delta_j \delta_t^{1/2}}{C_\delta \psi_0(0)} \sum_{j=j_1}^{j_2} \frac{\mathcal{R}\{W_n(s_j)\}}{s_j^{1/2}} \tag{5}$$

where the factor $\psi_0(0)$ is used for removes the energy scaling.

3.6 WAVELET COHERENCE ANALYSIS

The wavelet coherence, $R_n^2(s)$, is defined as the square of the cross-spectrum normalized by the individual power spectra [20].

$$R_n^2(s) = \frac{|S(s^{-1}W_n^{XY}(s))|^2}{S(s^{-1}|s^{-1}W_n^X(s)|^2) \cdot S(s^{-1}|s^{-1}W_n^Y(s)|^2)} \tag{6}$$

where $R_n^2(s) \in [0,1]$, $W_n^{XY}(s) = W_n^X(s) \times W_n^{Y*}(s)$ is the cross-wavelet, n represents the time index, s the scale of wavelet transform, $W_n^X(s)$ and $W_n^Y(s)$ are the wavelet transform of X and Y and S denotes the smoothing operator for $W_n^{XY}(s)$.

The wavelet phase difference or relative phase between two time series X and Y is given as:

$$\phi_n = \tan^{-1}(\mathcal{J}\{s^{-1}W_n^{XY}(s)\} / \mathcal{R}\{s^{-1}W_n^{XY}(s)\}) \tag{7}$$

where $\mathcal{J}\{.\}$ and $\mathcal{R}\{.\}$ are the imaginary and real parts of the wavelet spectra.

Wavelet coherence lies between 0 and 1. This reflects the time–scale variability of the linear relationship between two signals. A near-zero coherence indicates no linear relationship between the signals. Coherence close to 1 indicates a linear relationship between both signals.

4 RESULTS

Hierarchical Clustering on Principal Components Kasai basin rainfalls shows that the Kasai basin can be divided into three areas as in fig. 7.

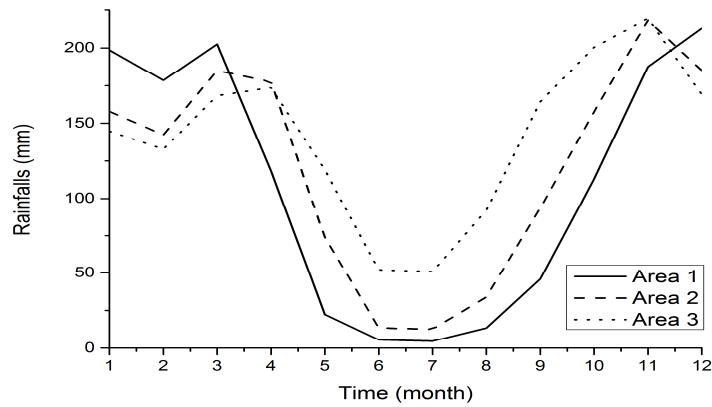


Fig. 6. Typology of rainfall regimes over the Kasai basin. Based on a hierarchical cluster analysis of mean monthly rainfall for 1940-1999 (SIEREM.v1data).

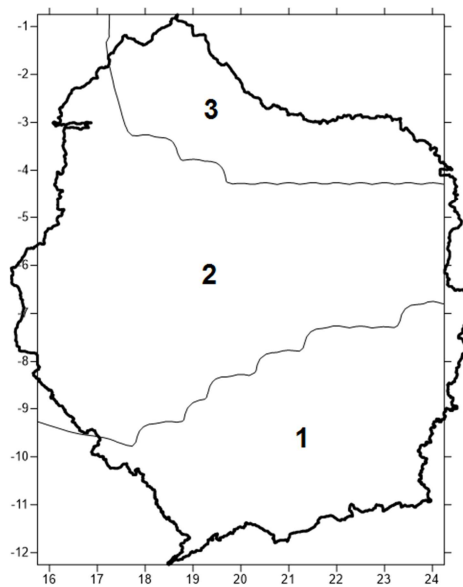


Fig. 7. Map of the 3 regional divisions of Kasai basin after hierarchical clustering methods on principal component analysis of rainfall

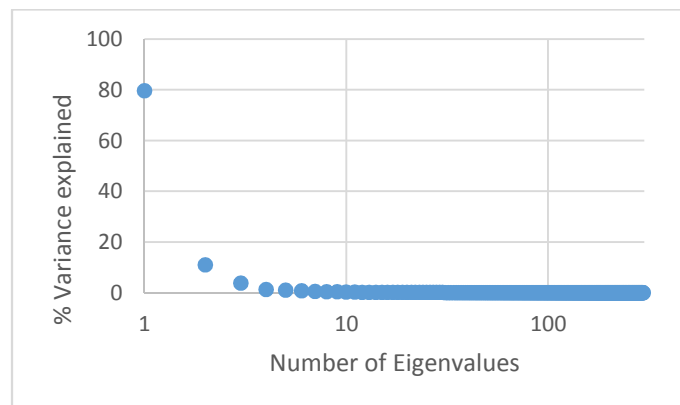


Fig. 8. Percentage of variance explained

Only PC1 will be discussed as it contributes for 80 % of the rainfall variability in the Kasai basin.

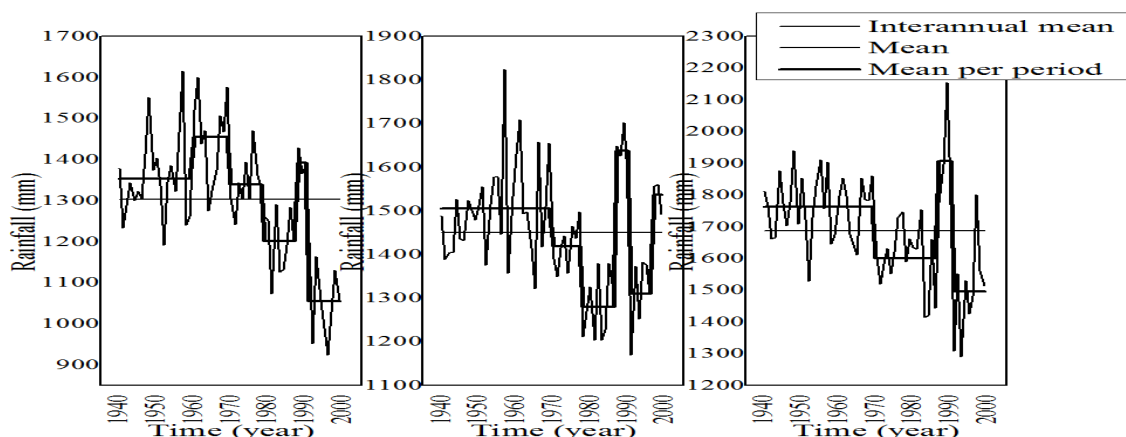


Fig. 9. Phases of homogeneous rainfalls over area 1,2 and 3 of Kasai basin (1940-1999)

By Hubert segmentation, which gives us the year of different ruptures observed on the rainfall time series (Fig. 9), we can see that rains on the Kasai basin are marked by fluctuations with a tendency on the one hand to the noticeable decline between 1970 and 1990, 1993 and 1999 and also an upward trend between 1960 and 1970 in area 1, 1990 and 1992.

The rain in area 1 presents five ruptures and therefore six times homogeneous rainfall:

- wet phases 1940-1959; 1959-1969; 1970-1979; 1988-1990;
- dry phases 1980-1987; 1991-1999;

The rain in area 2 presents five ruptures and therefore six times homogeneous rainfall:

- wet phases 1940-1969; 1988-1990; 1996-1999;
- dry phases 1970-1975; 1976-1987; 1991-1995;

The rain in area 3 presents three ruptures and therefore four times homogeneous rainfall:

- wet phases 1940-1959; 1970-1979;
- dry phases 1959-1969; 1980-1987;

4.1 IDENTIFICATION OF VARIABILITY MODES

The wavelet analysis is used to study the frequency composition and visualize unsteady fluctuations of hydro variables so as to identify the main modes of variability of flows and precipitation in the basin of the Kasai.

Table 1 shows the contribution of the energy bands in the discharge at Ilebo station and in rainfall in the Kasai basin.

The wavelet analysis of Kasai flow shows a plurality of energy bands (Figure 10 and 11):

- A period of about 1 year mainly expressed
- A band of 2-8 years well localized:
 - between 1953 and 1973 for both rainfalls and discharge;
 - between 1973 and 1995 for rainfalls
- A band of 8-16 years with a structure which begin around 1973 till 1999.

One can find a change point around 1970 (Figure 9 and 10) which is associated to low rainfalls and discharge.

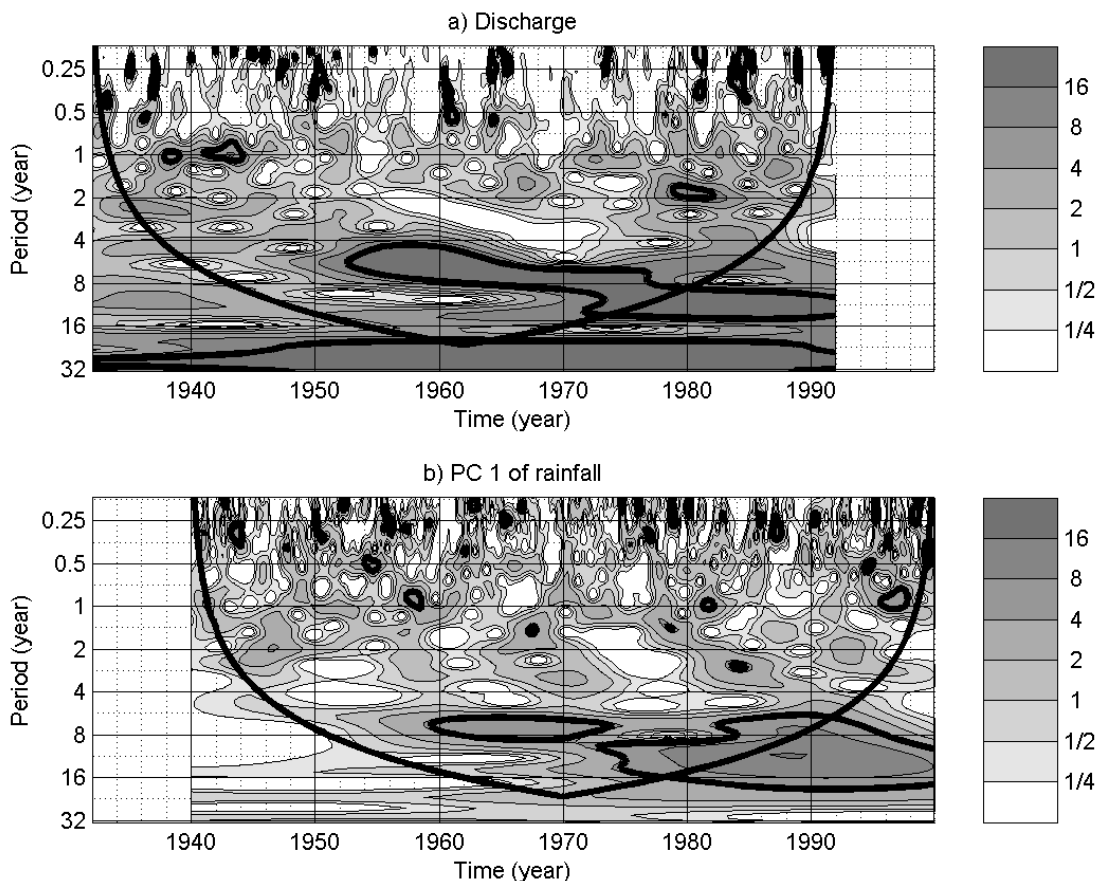


Fig. 10. Continuous wavelet power spectrum of a) discharge of Kasai River at Ilebo station and b) PC 1 of gridded rainfall over Kasai basin. The left axis is the Fourier period (in yr) corresponding to the wavelet scale on the right axis. The bottom axis is time (yr). The thick black contour designates the 5% significance level against red noise and the cone of influence (COI) where edge effects might distort the picture is shown as a lighter shade.

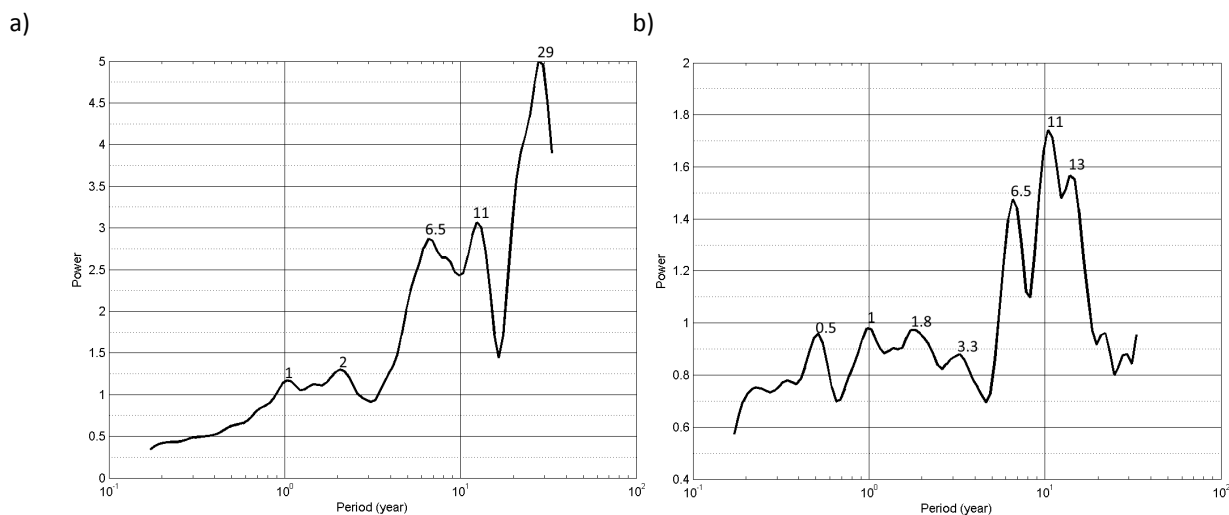


Fig. 11. Map of the 2 regional divisions of Kasai basin after hierarchical clustering methods on principal component analysis of rainfall

Table 2. Contribution of selected energy bands on total variance of discharges for the Kasai River at Ilebo station and rainfalls in Kasai basin

	Discharge	Rainfall		
	Ilebo	Region 1	Region 2	Region 3
0-1 year	42%	44%	45%	45%
1-2 years	34%	35%	30%	25%
2-8 years	10%	5%	6%	8%
8-16 years	6%	3%	4%	6%

4.2 COHERENCE BETWEEN RAINFALLS AND DISCHARGES

The discharge of Kasai River at Ilebo station seems to be strongly related to the rainfalls with total coherence around 59.63%. Figure 12 attests that the coherence between discharge and rainfall in the Kasai basin are essentially distributed across one year cycle and in 2-8 band (6.5 years).

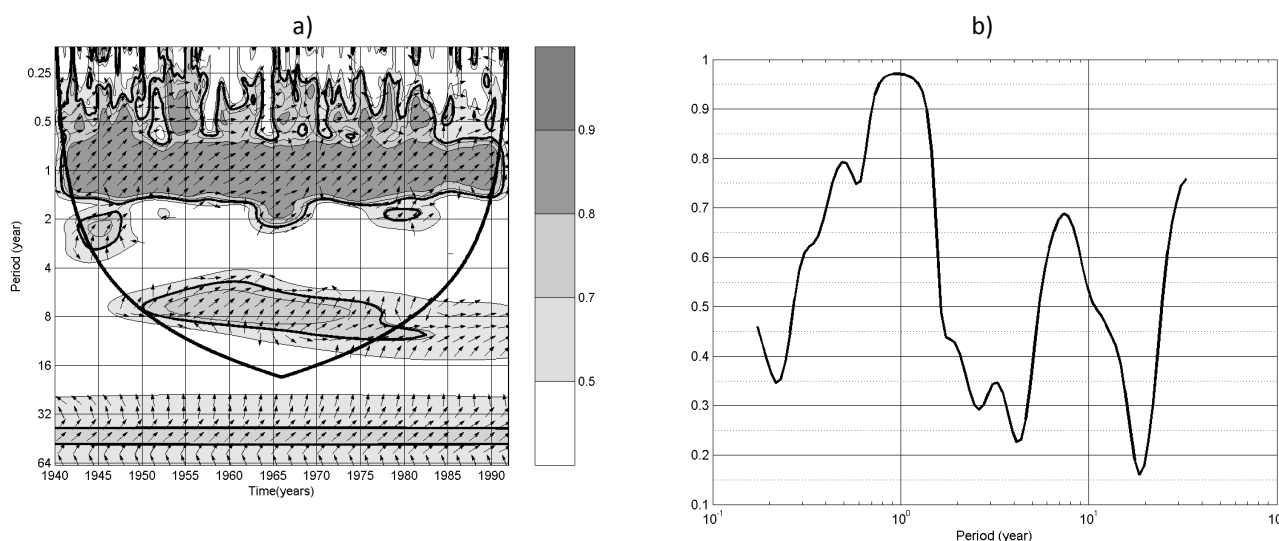


Fig. 12. Wavelet coherence between the discharge of Kasai River at Ilebo station and the PC 1 (80%) of rainfalls over Kasai basin. The 5% significance level against red noise is shown as a thick contour. The relative phase relationship is shown as arrows (with in-phase pointing right, anti-phase pointing lefting straight down).

4.3 RELATIONSHIP TO CLIMATE FORCING

Some characteristic oscillations were next related to several well-known climate indices. The coherence wavelet analyses between discharge time series at Ilebo station, rainfalls (Figure 12) in the three area of Kasai basin and climate index (NAO, NINO 3.4, TNA, TSA, DMI and Solar flux) show period of high coherence during some periods listed in table 2 and 3. Figure 13 and 14 also shows the characteristic periods of high wavelet coherence between discharge at Ilebo station, first principal component of rainfalls in Kasai basin and selected climate indices.

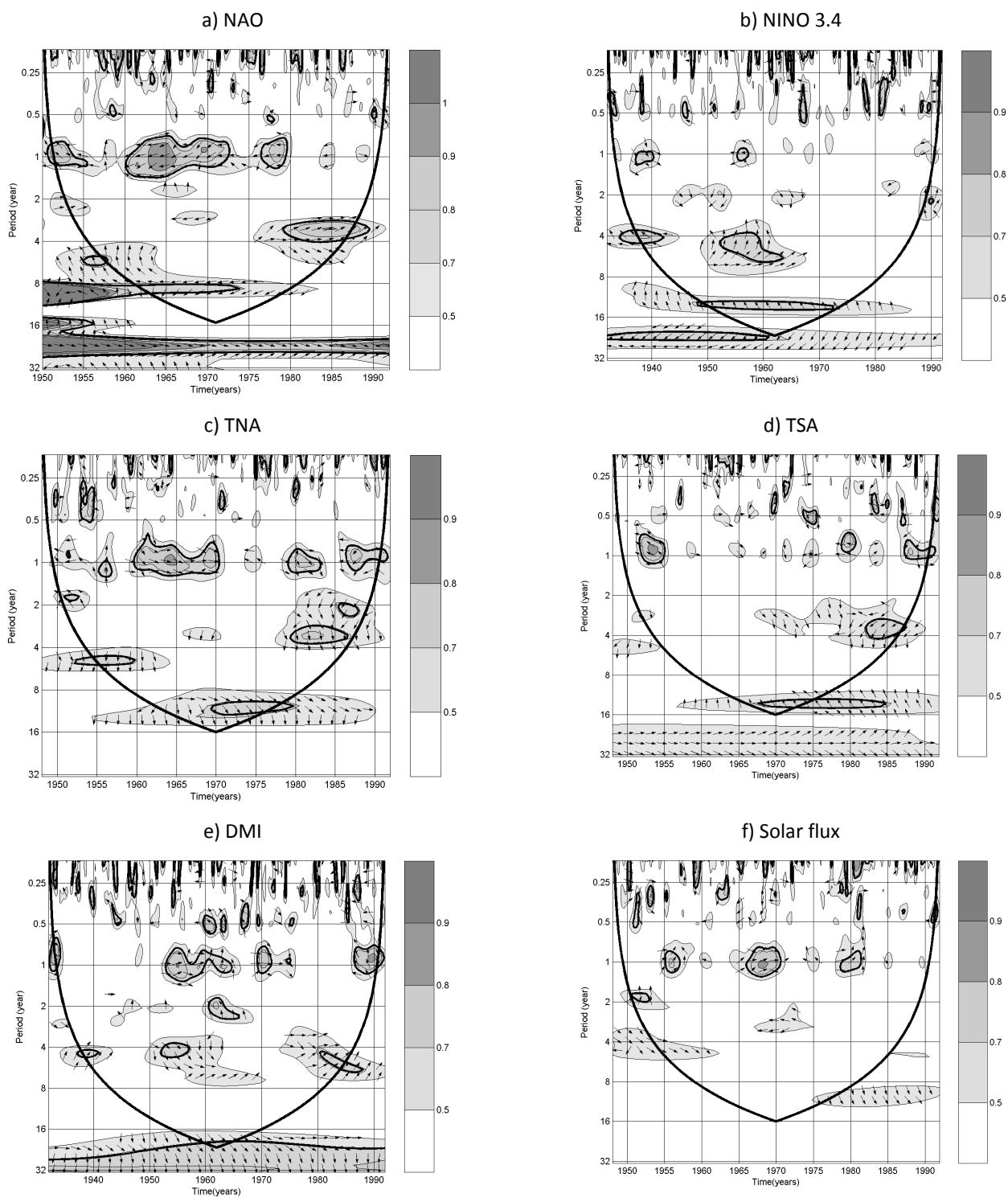
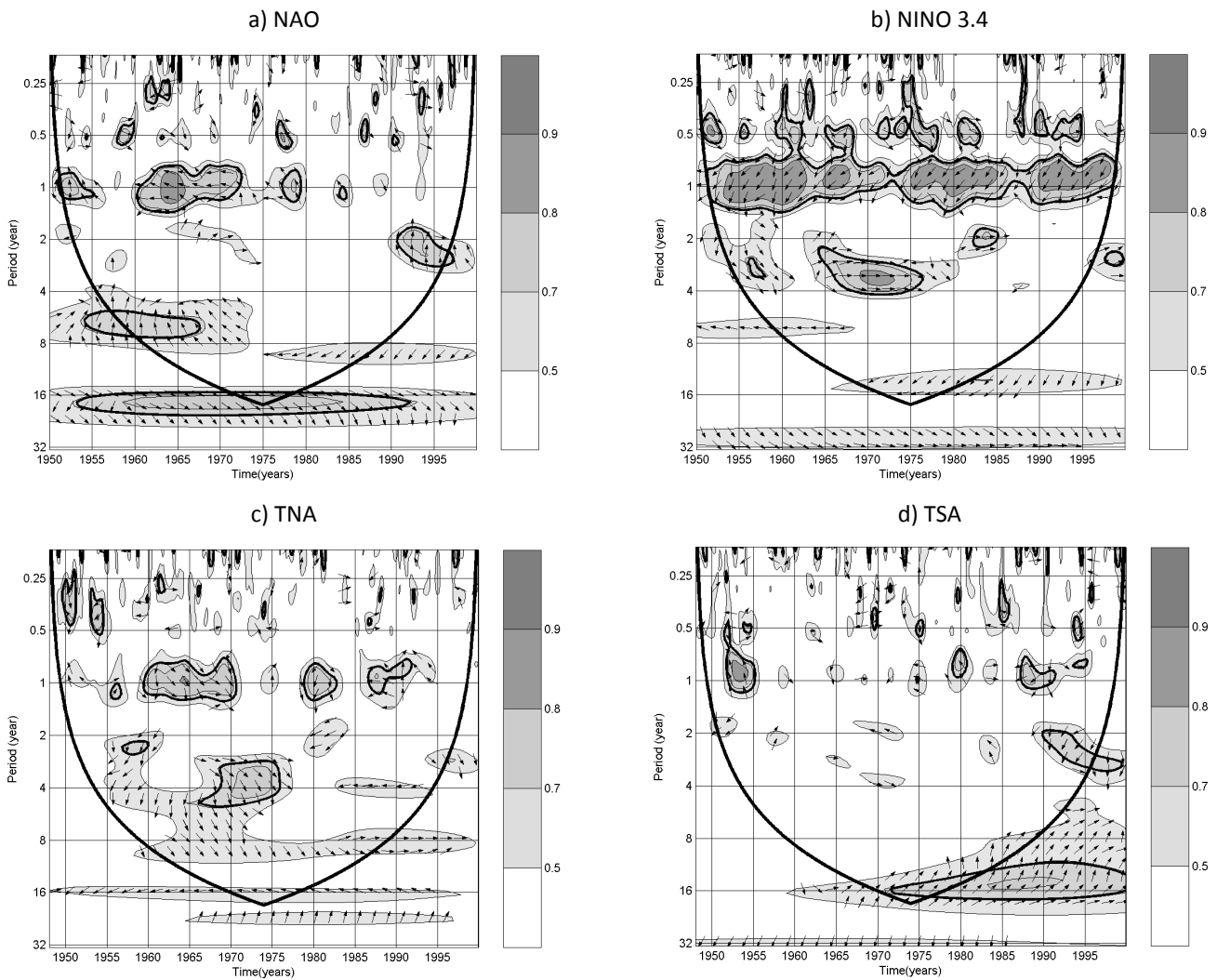


Fig. 13. Wavelet coherence between the discharge of Kasai River at Ilebo station and climate indices (NAO, Nino 3.4, TNA, TSA, DMI, Solar flux). The 5% significance level against red noise is shown as a thick contour.

Table 3. Contribution of selected energy bands on total variance of discharges for the Kasai River at Ilebo station and rainfalls in Kasai basin

Observed scales	NAO	Nino 3.4	TNA	TSA	DMI	Solar
2-4 years	1951-1955 1965-1971 1979-1990		1982-1987	1982-1987	1960-1969	
4-8 years	1955-1958	1932-1945 1952-1962			1950-1957 1980-1990	1948-1962
8-16 years	1950-1960	1948-1972	1967-1985	1967-1985		



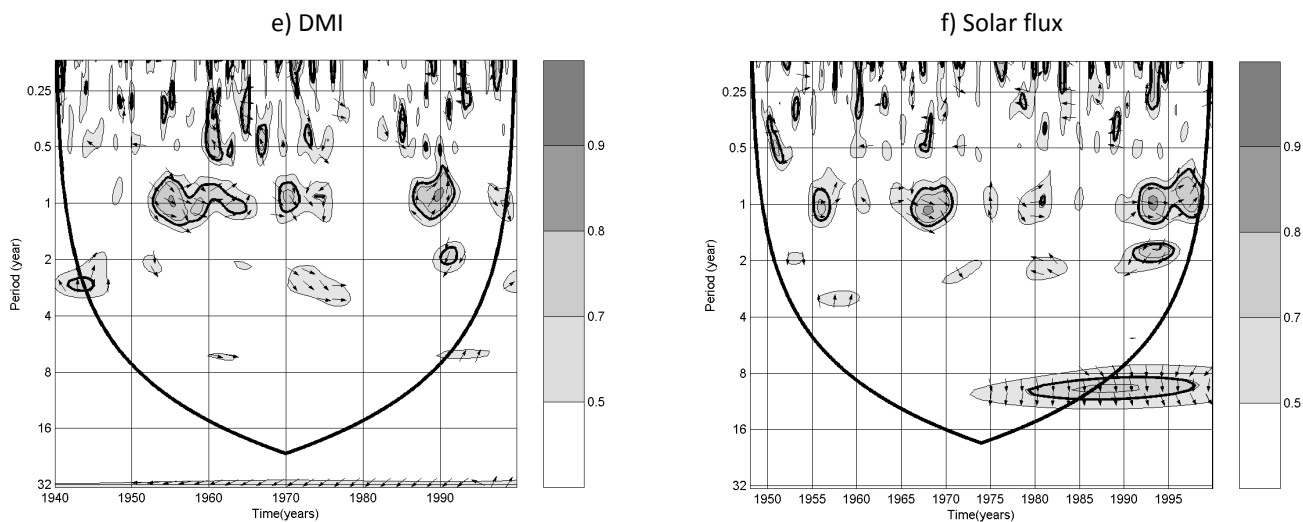


Fig. 14. Wavelet coherence between the PC 1 of rainfalls over Kasai basin and climate indices (NAO, Nino 3.4, TNA, TSA, DMI, Solar flux. The 5% significance level against red noise is shown as a thick contour. The relative phase relationship is shown as arrows (with in-phase pointing right, anti-phase pointing left, and BMI leading AO by 90° pointing straight down).

Table 4. Contribution of selected energy bands on total variance of discharges for the Kasai River at Ilebo station and rainfalls in Kasai basin

Observed scales	NAO	Nino 3.4	TNA	TSA	DMI	Solar
2-4 years		1955-1957 1964-1975	1957-1960 1967-1976 1979-1984 1982-1992	1990-1999	1940-1948 1951-1952 1970-1978	1956-1961
4-8 years	1954-1967	1950-1967	1962-1972			
8-16 years	1975-1995	1967-1999	1957-1999	1972-1999		1980-1997

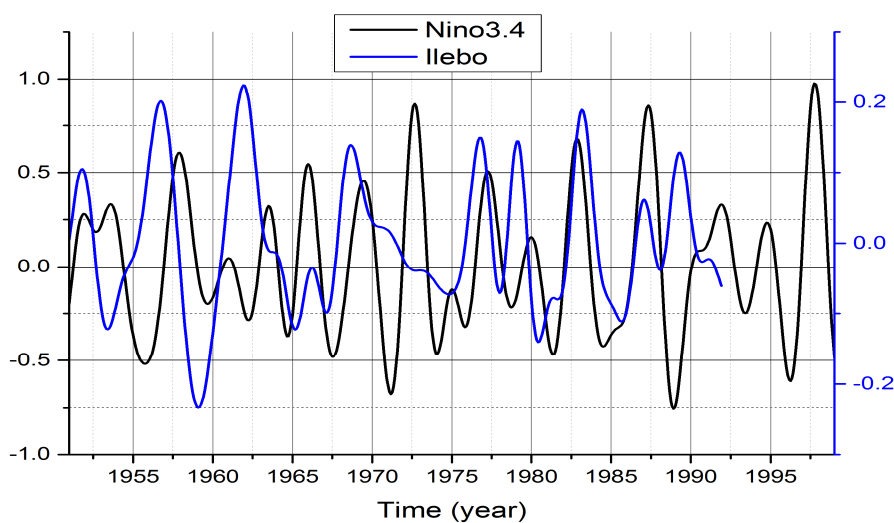


Fig. 15. Comparison between the wavelet –filtered reconstructions of the monthly discharge over 2-8 band-passed of Kasai river at Ilebo station and Nino 3.4 index.

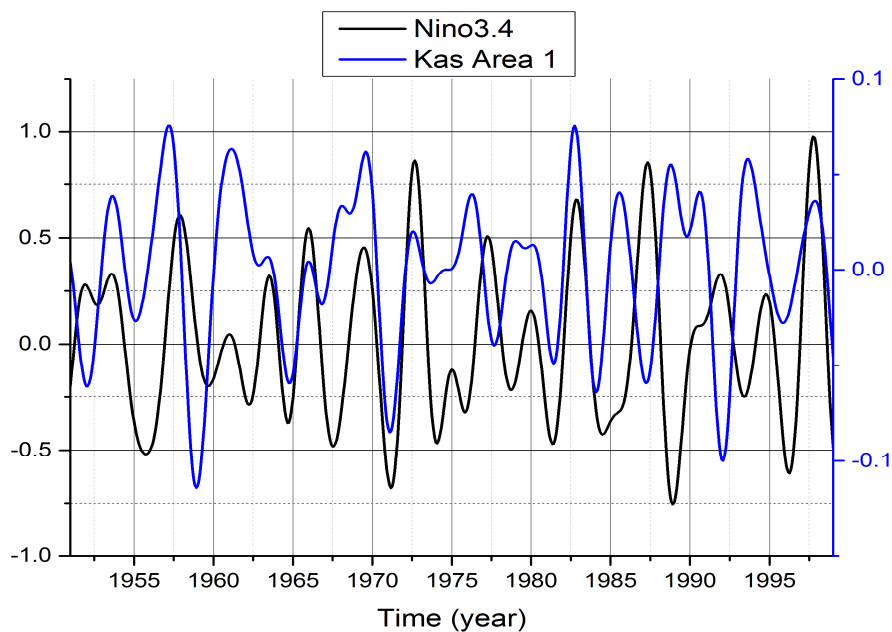


Fig. 16. Comparison between the wavelet –filtered reconstructions of the monthly rainfall over 2-8 band-passed on area 1 of Kasai basin and Nino 3.4 index.

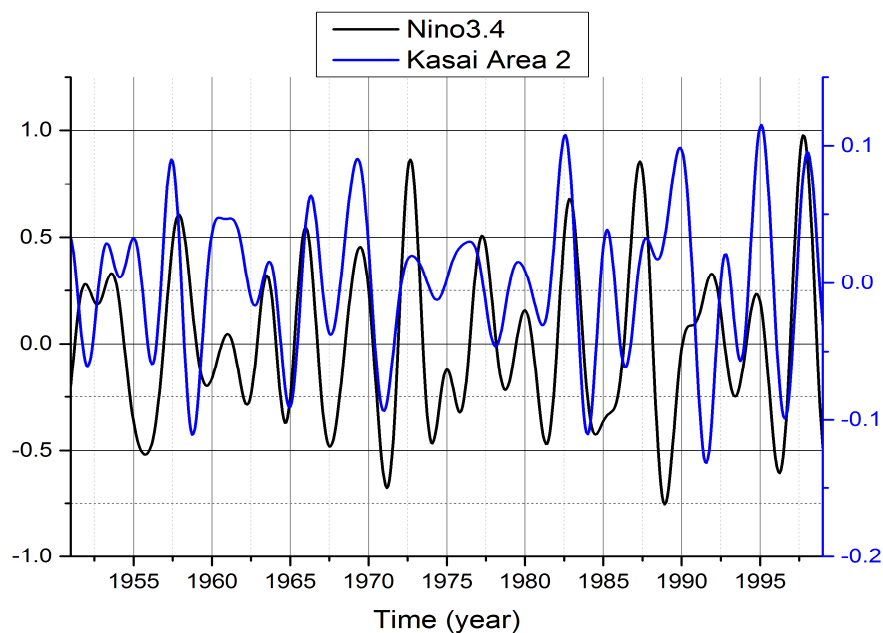


Fig. 17. Comparison between the wavelet –filtered reconstructions of the monthly rainfall over 2-8 band-passed on area 2 of Kasai basin and Nino 3.4 index.

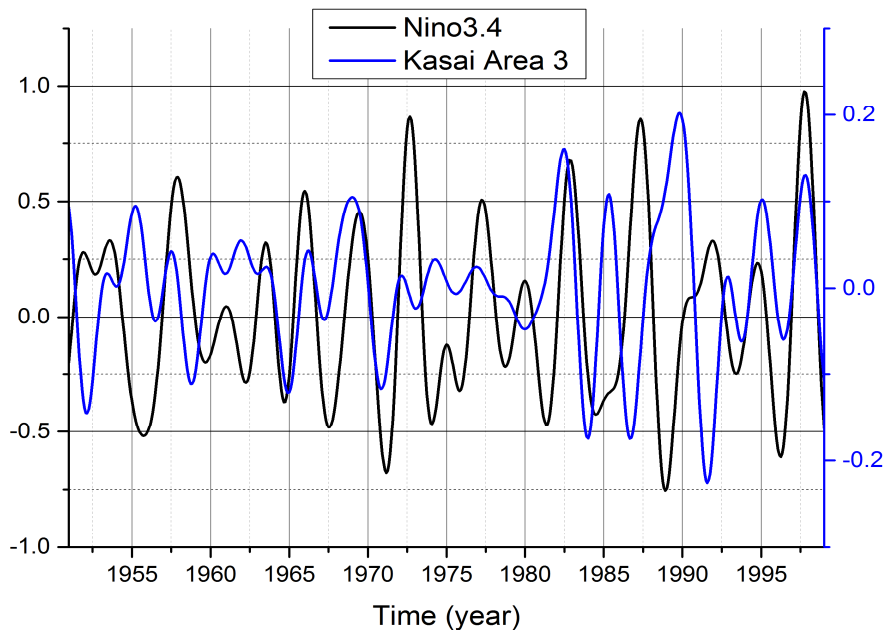


Fig. 18. Comparison between the wavelet-filtered reconstructions of the monthly rainfalls over 2-8 band-passed on area 3 of Kasai basin and Nino 3.4 index.

Figure 19 presents the relationships over the 2–8-yr band between the first principle component of the gridded rainfall over Kasai basin and the Niño3.4 SST index.

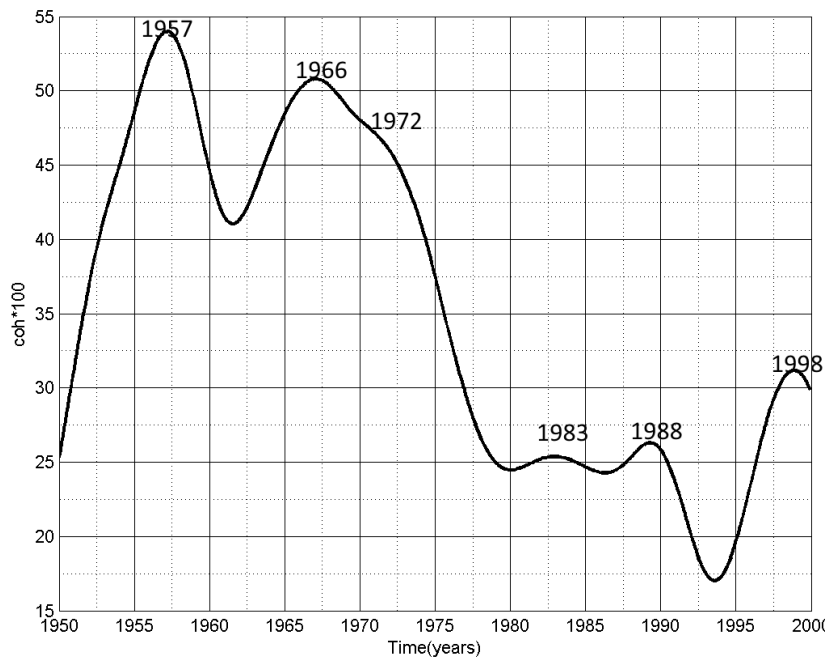


Fig. 19. Percentage of scale-averaged wavelet coherence over the 2–8-yr band for the gridded rainfall over Kasai basin and the Niño 3.4 SST index.

Mean percentage of wavelet coherence between discharge at Ilebo station or rainfall and some selected climate indices except Nino 3.4 index shows a weak nonlinear relationship (figure 20).

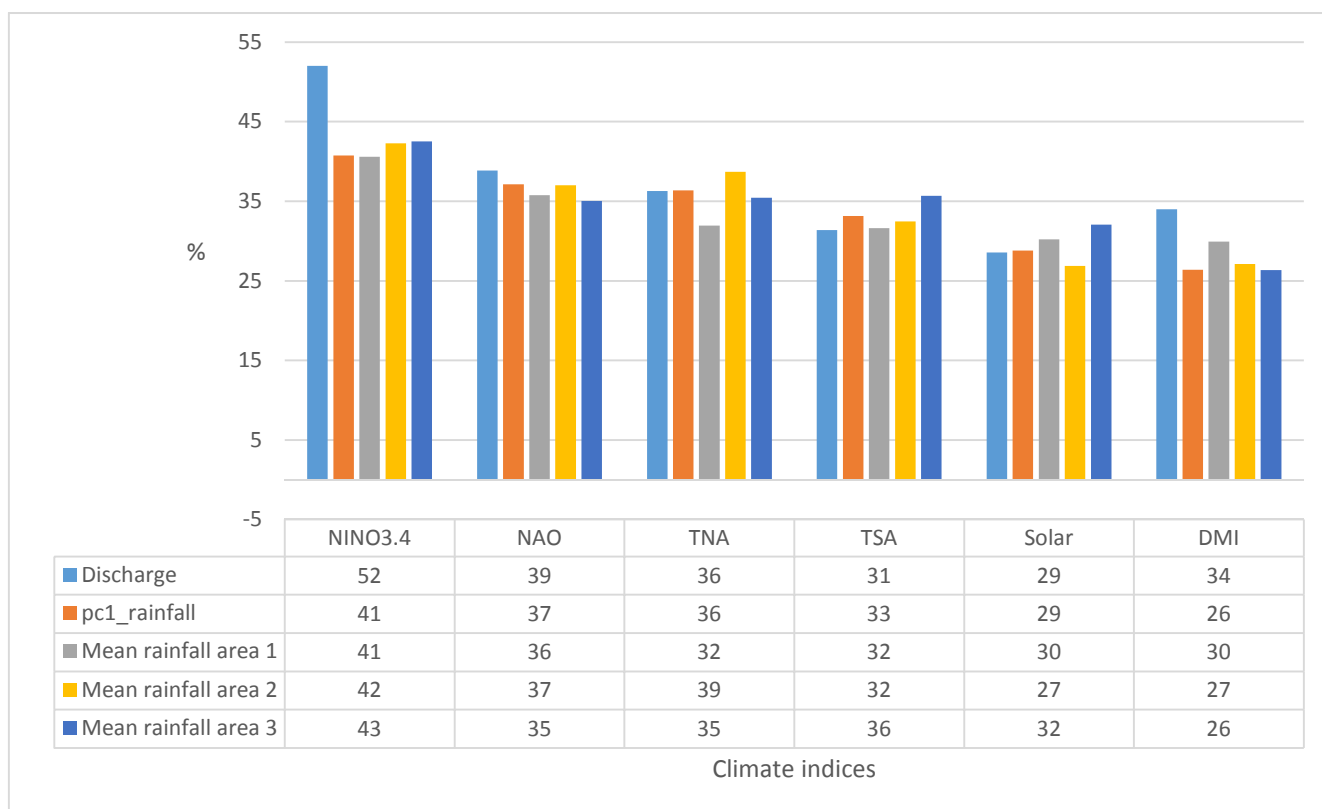


Fig. 20. Mean percentage of wavelet coherence (2-8 years band-passed) between of Ilebo’s discharge, PC 1 of gridded rainfalls, Monthly mean rainfalls in Kasai’s area 1, area 2, area 3 and some climate indices (NAO, NINO 3.4, TNA, TSA, DMI and Solar flux)

5 DISCUSSIONS AND CONCLUSION

We propose in this article a time-scale analysis of the river discharge fluctuations at Ilebo and rainfalls over the Kasai basin. The two temporal discontinuities around 1970-1975 and 1990-1995 over figure 9 and 10 were also found in other studies [8], [21]. The wavelet coherence between discharges at Ilebo and rainfall over Kasai River shows a high correlation in annual and the 2-8 year band –passed. Wavelet coherence between discharges at Ilebo and rainfall over Kasai River and selected climate index confirm a less (figure 20) and nonlinear relationship between the hydrology of the Kasai basin and the Pacific, Atlantic and Indian SST fluctuations. One can see covariability between rainfalls in the Kasai basin and ENSO phenomenon, particularly at El Niño years [10] (Figure 15-19). The influence of teleconnections is low but their effects seem especially important having regard to the covariability observed with El Niño example. Further investigations should be conducted to understand the variability of the Kasai river basin regime variability. What is the role of deforestation and of human activity and urbanization on water resource to availability?

ACKNOWLEDGMENTS

Thanks for the gridded rainfall data providers IRD and HydroSciences Montpellier, France. The wavelet software was provided by:

- Torrence and Compo at <http://atoc.colorado.edu/research/wavelets/>
- A. Grinsted at <http://www.pol.ac.uk/home/research/waveletcoherence/>

REFERENCES

- [1] D. Backer, "La rivière Kasai entre Kwamouth et Port - Francqui. L'amélioration de ses conditions de navigabilité par balisage, signalisation et travaux d'aménagement," *bulletin des séances de l'Institut Royal Colonial Belge*, vol. III, no. 1, pp. 252 - 278, 1932.
- [2] Devroey and E. , Le Kasai et son bassin hydrographique, Goemaere, 1939.
- [3] Ntombi and Kisangala, "Impact de la lithologie et de l'hydrométrie sur la navigabilité du Kasai en R. D. Congo," *Annales de la Faculté des Sciences*, pp. 157-164, 2002.
- [4] Kisangala and Ntombi, "Estimation des réserves régulatrices et établissement de la courbe de tarissement du bassin versant du Kasai durant la période d'étiage à l'échelle de Lumbu," *Revue Congolaise des Sciences Nucléaires*, vol. 26, no. 2, 2012.
- [5] J.-F. Boyer, C. Dieulin, N. Rouché, A. Cres, E. Servat, J.-E. Paturel and G. Mahé, "SIEREM : an environmental information system for water resources," in *Climate variability and change : hydrological impacts*, vol. 308, P. -. AISH and 308, Eds., Wallingford (GBR) ; Paris, AISH ; UNESCO, 2006, pp. 19--25.
- [6] N. Rouché, G. Mahé, S. Ardoin-Bardin, B. Brissaud, J.-F. Boyer, A. Crès, C. Dieulin, G. Bardin, G. Commelard, A. Dezetter, J.-E. Paturel and É. Servat, "Constitution d'une grille de pluies mensuelles pour l'Afrique (période 1900-2000)," *Sécheresse*, vol. 11, no. 1, 2010.
- [7] G. Mahé, «Modulation annuelle et fluctuations interannuelles des précipitations sur le bassin-versant du Congo,» chez *Actes du Colloque PEGI Grands Bassins Fluviaux Péri-Atlantiques : Congo, Niger, Amazone, INSU, CNRS, ORSTOM, 22-24 nov. 1993*, Paris, 1995.
- [8] G. Mahe, Y. L'Hote, J. Olivry and G. Wotling, "Trends and discontinuities in regional rainfall of West and Central Africa: 1951–1989," *Hydrological Sciences Journal*, vol. 46, pp. 211-226, 2001.
- [9] J. W. Hurrell, "Decadal Trends in the North Atlantic Oscillation: Regional Temperatures and Precipitation," *Science*, vol. 269, no. 5224, pp. 676-679, 1995.
- [10] K. E. Trenberth, "The definition of el nino," *Bulletin of the American Meteorological Society*, vol. 78, pp. 2771-2777, 1997.
- [11] D. Enfield and E. Alfaro, "The dependence of Caribbean rainfall on the interaction of the tropical Atlantic and Pacific oceans," *Journal of Climate*, vol. 12, p. 2093–2103, 1999.
- [12] "Latest Solar Radio Flux Report from DRAO, Penticton," Natural Resources Canada, 10 february 2016. [Online]. Available: <http://www.spaceweather.ca/solarflux/sx-4-en.php>.
- [13] K. Ashok, Z. Guan and T. Yamagata, "Impact of the Indian Ocean dipole on the relationship between the Indian monsoon rainfall and ENSO," *Geophysical Research Letters, Wiley Online Library*, no. 28, pp. 4499-4502, 2001.
- [14] S. Le Dien and J. Pagès, "Hierarchical Multiple Factor Analysis: application to the comparison of sensory profiles," *Food Quality and Preference*, vol. 14, p. 397–403, 2003.
- [15] L. Lebart, A. Morineau and K. Warwick, *Multivariate descriptive statistical analysis*, Wiley, 1984.
- [16] P. Hubert, J. P. Carbonnel and A. Chaouche, "Segmentation des séries hydrométéorologiques-application à des séries de précipitations et de débits de l'Afrique de l'ouest," *Journal of hydrology, Elsevier*, vol. 110, pp. 349-367, 1989.
- [17] C. Torrence and G. Compo, "A practical guide to wavelet analysis," *Bull. Am. Meteorol. Soc.*, vol. 79, pp. 61-78, 1998.
- [18] M. Farge, "Wavelet transforms and their applications to turbulence," *Annual Review of Fluid Dynamics*, vol. 24, pp. 395-457, 1992.
- [19] Y. Hao, G. Liu, H. Li, Z. Li, J. Zhao and T. Yech, "Investigation of karstic hydrological processes of Niangziguan Springs (North China) using wavelet analysis," *Hydrol. Process*, vol. 26, pp. 3062-3069, 2012.
- [20] C. Torrence and P. Webster, "Interdecadal changes in the ENSO-monsoon system," *J. Climate*, vol. 12, pp. 2679-2690, 1999.
- [21] A. Laraque, G. Mahe', D. Orande and B. Marieu, "Spatiotemporal variations in hydrological regimes within Central Africa during the XXth century," *Journal of Hydrology*, vol. 245, p. 104–107, 2001.